Effect of carbon nanotube (CNT) content on the hardness, wear resistance and thermal expansion of in-situ reduced graphene oxide (rGO)-reinforced aluminum matrix composites

Peter Nyanor[1], Omayma El-Kady[2], Hossam M. Yehia[3], Atef S. Hamada[1, 4], Koichi Nakamura[1,5], Mohsen A. Hassan[1, *]

[1] Egypt-Japan University of Science and Technology, Department of Material Science and Engineering, Alexandria, Egypt;

[2] Powder Technology Division, Central Metallurgical Research and Development Institute, Cairo, Egypt,

[3] Mechanical Engineering Department, Faculty of Industrial Education, Helwan University, Egypt.

[4] University of Oulu, Kerttu Saalasti Institute, Pajatie 5, FI-85500 Nivala, Finland

[5] Center for the Promotion of Interdisciplinary Education and Research, Kyoto University, Kyoto 615-8540, Japan

Abstract

Aluminum matrix composites reinforced with reduced graphene oxide (rGO) and hybrid of carbon nanotube (CNT) and rGO are fabricated by solution coating powder metallurgy process. The hardness, wear resistance and coefficient of thermal expansion (CTE) of the reinforced aluminum composites and the associated microstructural changes with rGO range (0.2-0.6 wt. %) and hybrids of 0.2 wt. % CNT-rGO at different ratios have been investigated. The intensive microstructural observations show that rGO is adsorbed on Al particles and uniformly distributed in the Al matrix composites.

The hardness values of the composites increase significantly with rGO reinforcement exhibiting the maximum hardness at 0.4 wt. % rGO. Compared with the hybrid composites CNT-rGO/Al counterparts fabricated by the same route and wt. percent of 0.2, the hardness values in the hybrid CNT-rGO increase considerably. Similar to the hardness, the results of wear tests also exhibit corresponding variation in the values of the wear rates. The improvement in the wear resistance of the hybrid CNT-rGO/Al composite is pronounced in this work. Whereas the rGO reinforcements decrease significantly the wear rate of the aluminum-base by 98%, the wear resistance of the corresponding hybrid CNT-rGO is significantly higher than that of the preceding composites. Maximum CTE reduction of 28% was recorded for hybrid CNT-rGO (1:1) reinforced composite.

Keywords: Aluminum matrix composite; Hybrid CNTs-graphene oxide; Wear resistance; Hardness; Powder metallurgy

*Correspondence: Mohsen A. Hassan, Email: mohsen.khozami@ejust.edu.eg; Tel.: +201024904983

1. Introduction

Aluminum matrix composites (AMCs) are the most commonly used metal matrix composite (MMC) in automotive and aerospace applications [1]. About 20 to 25 percent of companies use aluminum-based matrix [2]. The aluminum-based MMCs have major advantages in strength, weight reduction, improved stiffness, better thermal properties, improved electrical performance, thermal or heat management, improved thermal expansion coefficient, etc. in comparison to unreinforced monolithic material [3–5]. Unfortunately, aluminum has some disadvantages such as low strength, high wear rate and high coefficient of thermal expansion (CTE) which is very important in automobile components [6]. Consequently aluminum must be reinforced with a ceramic material that have high strength, high wear resistance and low CTE. It is well known that reduced graphene oxide (rGO) and carbon nanotube (CNT) reinforcements are ceramic materials with superior mechanical properties and thermal stability [7].

CNTs and graphene which are allotropes of graphite have been used in reinforcing almost all matrix material types; polymer [8], metals [9] and ceramics [10]. These composites are reported to exhibit extraordinary improvement in properties. Recently, hybrid reinforcement of CNTs and graphene is fast gaining attention due to the synergistic improvement in composite properties. This means the hybrid reinforced composite properties are significantly superior to CNT or graphene composites with same reinforcement volume fraction as demonstrated by Li et al [11]. The contribution of each reinforcement, strengthening mechanism, interaction between CNTs and graphene and the ratio of CNT:graphene needed for synergistic improvement to occur are still subject of interest to researchers.

The preferred method of CNT and graphene dispersion is the conventional ball milling which is reported to cause damage to the CNTs and graphene sheets [12,13]. The powder metallurgy (PM) route remains the most effective fabrication process for metal matrix composites. Al matrix composites with graphene content of 0.3 wt.% were fabricated by Wang et al. [14] and Rashad et al. [15] using ball milling and PM with increased yield strength of 249 MPa and 195 MPa respectively. The highest graphene content reported is 1 wt.% using ball milling as the main dispersion method. For instance, Kwon et al. [16] dispersed GO by high energy ball milling to double the tensile strength (540 MPa) and Vickers hardness (166 HV) of $AlMg_5$ alloy with 1 vol.% GO over the unreinforced $AlMg_5$ alloy fabricated by similar method, while the strength quadrupled to a value of 800 MPa. Graphene reinforced Al matrix composites were fabricated by PM technique at sintering temperature of 600 °C under 25 MPa pressure. The ultimate tensile strength (UTS) of the composites increased to about 30% higher than that of pure Al with increasing graphene content up to 0.3 wt.% but declined with further increase in graphene content. The strain however decreased gradually with increasing graphene content [17].

The focus of research into graphene and hybrid CNT-graphene reinforced Al matrix composites have been mainly on improvement of fabrication methods, characterization and tensile property [18–21]. Despite the success in homogeneous dispersion of graphene in Al matrix, the effective mass fraction of graphene reinforcement has been limited to about 3 wt.%. To further harness the reinforcing potential of graphene, combination with CNT to form hybrid reinforcement is promising. Until now, only few researchers have studied hybrid CNT-rGO reinforced Al matrix composites [11,22]. Therefore, there is the need to further study rGO reinforced Al matrix composites and optimize the ratio of CNT:rGO reinforcement to achieve the maximum synergistic effect in aluminum composites.

In the present work, solution coating of Al particles with GO and hybrid CNT-GO has been achieved by in-situ reduction of GO on Al particle surfaces. The resulting composite powders were compacted and sintered in a vacuum furnace. The hardness, wear resistance and CTE properties of the fabricated Al composites have been studied. The morphology of raw powders and prepared composites are carefully studied in order to fully understand and interpret the enhanced properties

2. Experimental procedures

2.1 Preparation of powder mixtures

In the present work, the aluminum powder (average particle size of 10 μm, purity of 99.5 %) supplied by DOP Organik Kimya Ltd, Turkey, is used as matrix. Graphene oxide (GO) was synthesized using the modified Hummers' method from expandable graphite [23]. The CNTs reinforcement of ~13 nm in diameter and 1-2 μm in average length was used. Fig. 1 shows a schematic illustration of the composite fabrication process. Two different powder samples are prepared for this study; rGO and hybrid rGO-CNT coated aluminum particles. To prepare rGO/Al samples, 0.24 g of GO is weighed and transferred into 300 mL of deionized (DI) water. The GO is dispersed in the DI water by ultrasonication for 1 hr. The Al powder particles are cleaned by acetone using mechanical stirring for 5 mins, and then dried. Al slurry is prepared with 0.2 wt.%, 0.4 wt.% and 0.6 wt.% GO by adding 20 g of Al powder to 50 ml, 100 ml and 150 ml of GO solution respectively. DI water was added to increase mixture volume to 200 ml. The resulting slurries are stirred using a magnetic stirrer at 420 rpm until GO is adsorbed unto Al particle surfaces, which is indicated by the solution becoming colourless and transparent as shown in Fig. 2a. It is expected that GO is in-situ reduced (rGO) on the surface of Al particles as reported by Zhang et al. [24] and Fan et al. [25]. The adsorption time is increased by increasing the rGO weight percent and decrease with increasing volume of DI water [26]. For instance, the adsorption time was 30 min, 50 min and 120 min for 0.2, 0.4 and 0.6 wt.% GO respectively. The rGO coated Al particles are strained and transferred into acetone. Magnetic stirring was done for about 5 min before the Al powder slurry is then filtered and dried at 60 °C for 1h.

Similarly, the hybrid CNT-GO coated Al particles are prepared by adding combined weight percentage of 0.2 GO and CNT in CNT:GO ratios (wt/wt) of 3:1, 1:1 and 1:3 to DI water. The hybrid CNT-GO/Al powder mixture is then prepared following the same procedure as described for GO/Al powder mixture. The CNTs are initially acid treated in H_2SO_4/HNO_3 mixture (3:1, v/v) by ultrasonication for 1 hr before being transferred slowly into the GO solution to facilitate uniform dispersion.

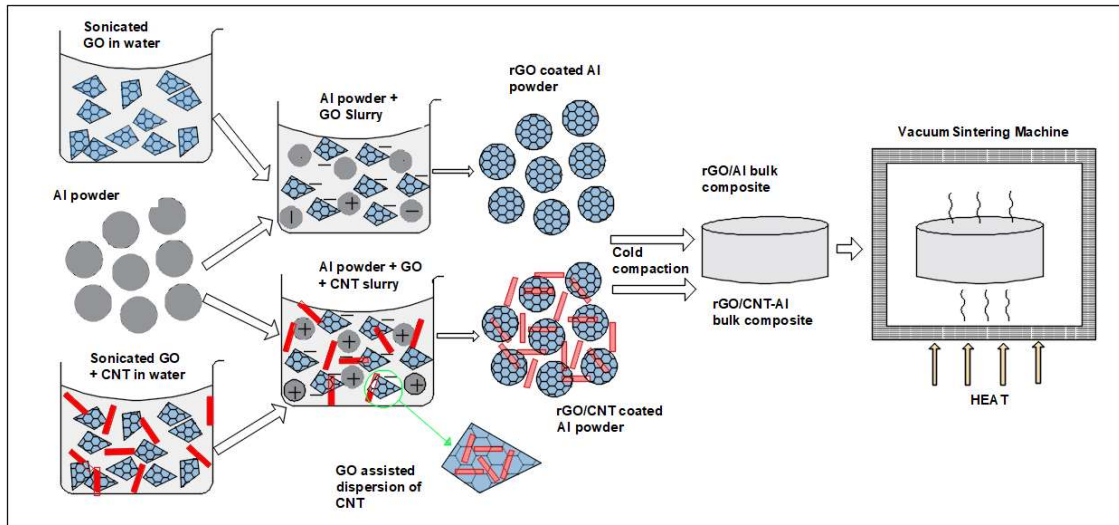**Fig. 1** Schematic illustration of solution coating of rGO and hybrid CNT-rGO on Al particles and fabrication of bulk composites

2.2 Consolidation of composites

The dry powder mixture (rGO/Al and CNT-rGO/Al) is prepared for cold compaction by adding 0.5 wt.% paraffin wax and heating at 100 °C for 30 min. The dried composite powders were compacted in a steel mold under a pressure of 500 MPa using a uniaxial hydraulic compaction machine. Subsequently, the compacted composite samples were vacuum sintered at 600 °C. Fig. 2b shows schematically the heating cycle used in sintering the compacted powder composites. The specimens are heated in vacuum at the rate of 5 °C/min to 250 °C and held for 15 min to facilitate removal of paraffin wax, in a step called dewaxing. The heating cycle is continued at a rate of 5 °C/min to 600 °C and soaked for 1 hour at this temperature before cooling. Samples of pure Al are also fabricated using the same conditions for comparison. The fabricated composite materials were coded according to the content of rGO in wt% and the ratio of CNT:rGO for hybrid reinforcements.
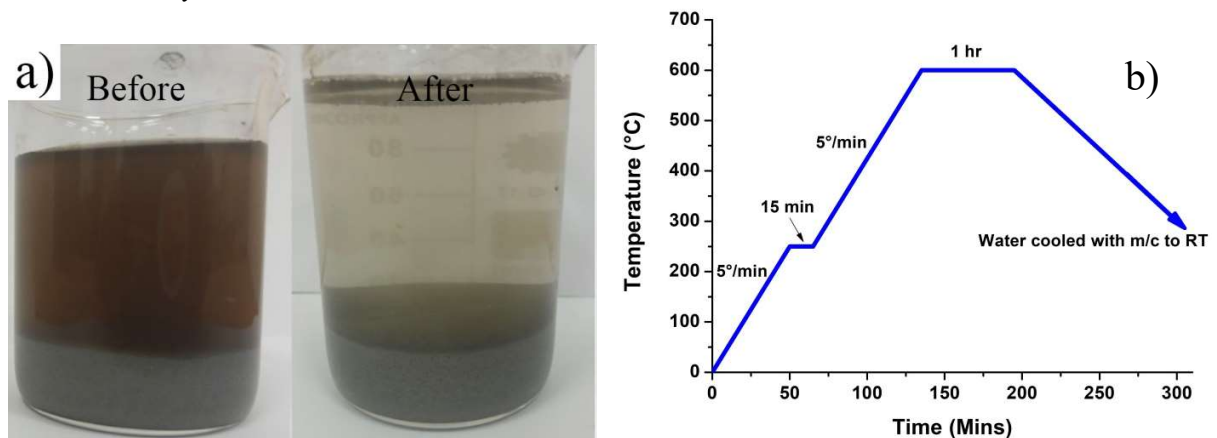

Fig. 2 (a) Photograph of Al powder in GO/CNT-GO solution before and after adsorption coating process (b) schematic illustration of the heating cycle used in sintering of composites

2.3 Characterization

The actual density of sintered composite samples was measured using Archimedes' principle according to ASTM D1217 standard. The theoretical densities were calculated using rule of mixtures (ROM).The densities of CNT, graphene and pure Al are taken as 2.2 g/cm3 [27], 1.06 g/cm3 [28] and 2.7 g/cm^3 respectively. Scanning electron microscope (JEOL JSM – 6010LV, Japan) and transmission electron microscopy (JEOL JSM – 2100F, Japan) were employed to observe the morphology of the carbon nanofillers, Al powder, composite powder mixtures and fabricated composites materials. X-ray diffraction (XRD) was used to analyze the constituent phase structure of sintered samples. A Shimadzu xlab 6100 diffractometer with Cu Kα radiation (V= 40 KV, I = 30 mA) at a scanning rate of 12°/min is used. Vickers hardness test measurement was conducted on the Shimadzu hardness tester HMV-2, Japan by applying a load of 1.96 N for a loading time of 10 s. The reported values correspond to the mean of five measurements. Dry sliding wear test was conducted using TNO Tribometer-block-on-ring wear test machine, ASTM G-77. The specimen dimensions prepared for wear testing are $7 \times 5 \times 12$ mm with its axis parallel to the pressing direction. The rotating sliding ring made of 63 HRC steel has 73 mm diameter. A speed of 200 rpm, and force of 10 N was applied for 10 min. The wear rate is determined from Eq. 1 as:

$$wear\ rate = \frac{w_1 - w_2}{T}\ g/sec \qquad (1)$$

where $w_1 and\ w_2$ are the weight of samples before and after wear test respectively, T is test time.

The CTE was measured by heating the samples from room temperature to 350 °C, using a system and technique described in details by Yahia *et al* [29].

3. Results and discussion

3.1 Microstructure analysis

Fig. 3 shows the SEM images of the as-received Al powder, rGO and CNT-rGO/Al composite powder prepared by solution coating. It can be observed that the Al powder has a near-spherical shape with relatively smooth surface as shown in Fig. 3(a). However, after the solution coating process on Al particles with different contents of rGO, the surface of Al powder is gradually homogenously coated with rGO, as shown by the change in surface texture in Fig. 3(b-c). Fig. 3d reveal the SEM images of hybrid CNT-rGO coated Al powder with CNT:rGO ratio (1:1). It is apparent from the SEM images that, the surface of hybrid CNT-rGO coated powder particles are slightly smoother than only rGO coated ones. CNTs could not be observed in these SEM images since they are expected to be covered by the rGO [30,31].

In Fig. 4(a-d), the SEM images of rGO reinforced Al composites are presented. The rGO appears as either continuous coating as indicated in red circle of Fig. 4b or as small particles on Al surfaces caused by polishing and etching. Significantly large amount of pores can be seen in the SEM image of 0.6rGO/Al composite (Fig. 4c,d), which can drastically reduce the density of the composite. A higher magnification in Fig. 4d shows a higher magnification of rGO on Al surfaces and presents of pores in the 0.6rGO/Al composite. Overall, it was observed that pores or

microvoids increased with increasing rGO content. The SEM could not reveal CNTs in the hybrid composites; therefore, TEM was employed to observe CNTs.
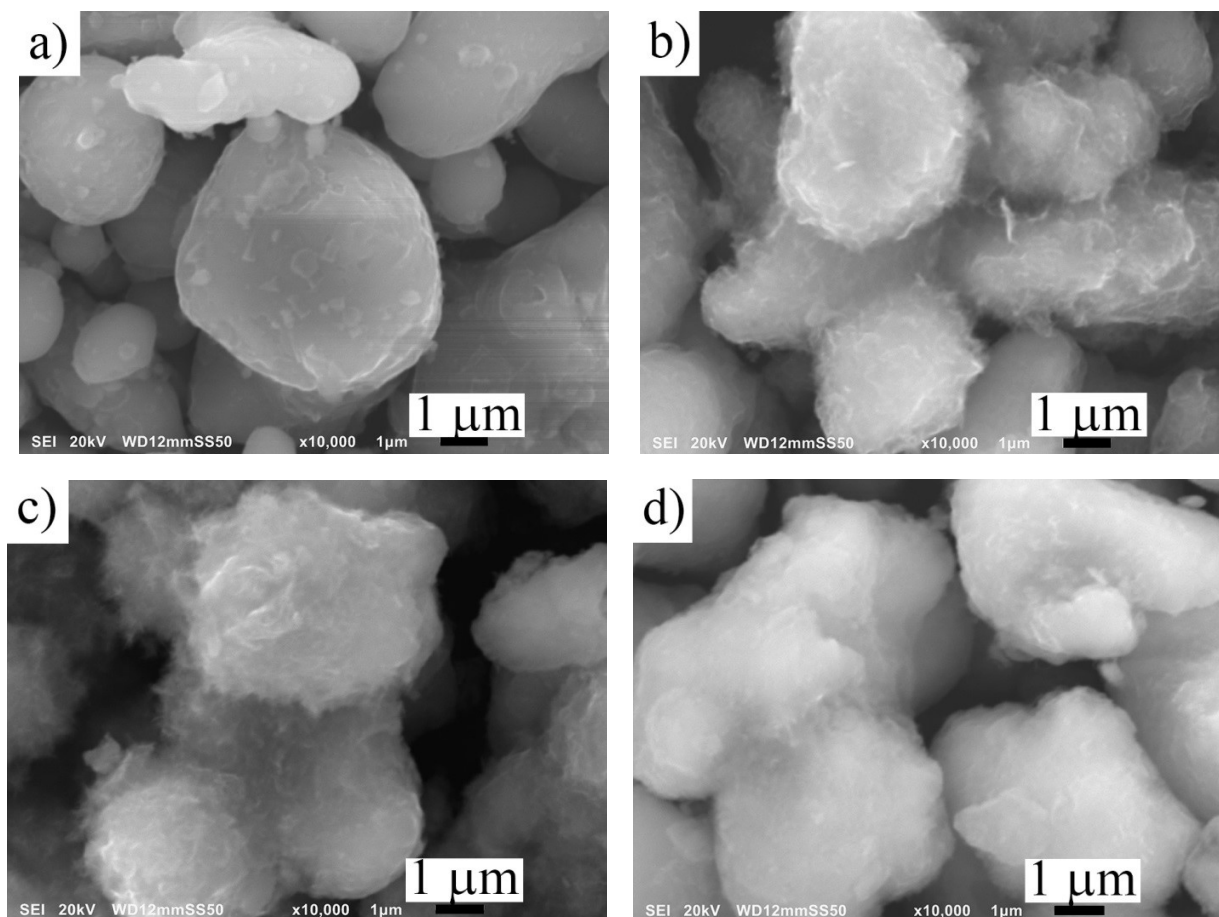

Fig. 3 Representative SEM image of coated Al powder (**a**) Pure Al powder (**b**) 0.4 wt.% rGO (**c**) 0.6 wt.% rGO (**d**) 0.2 wt.% CNT-rGO (1:1)
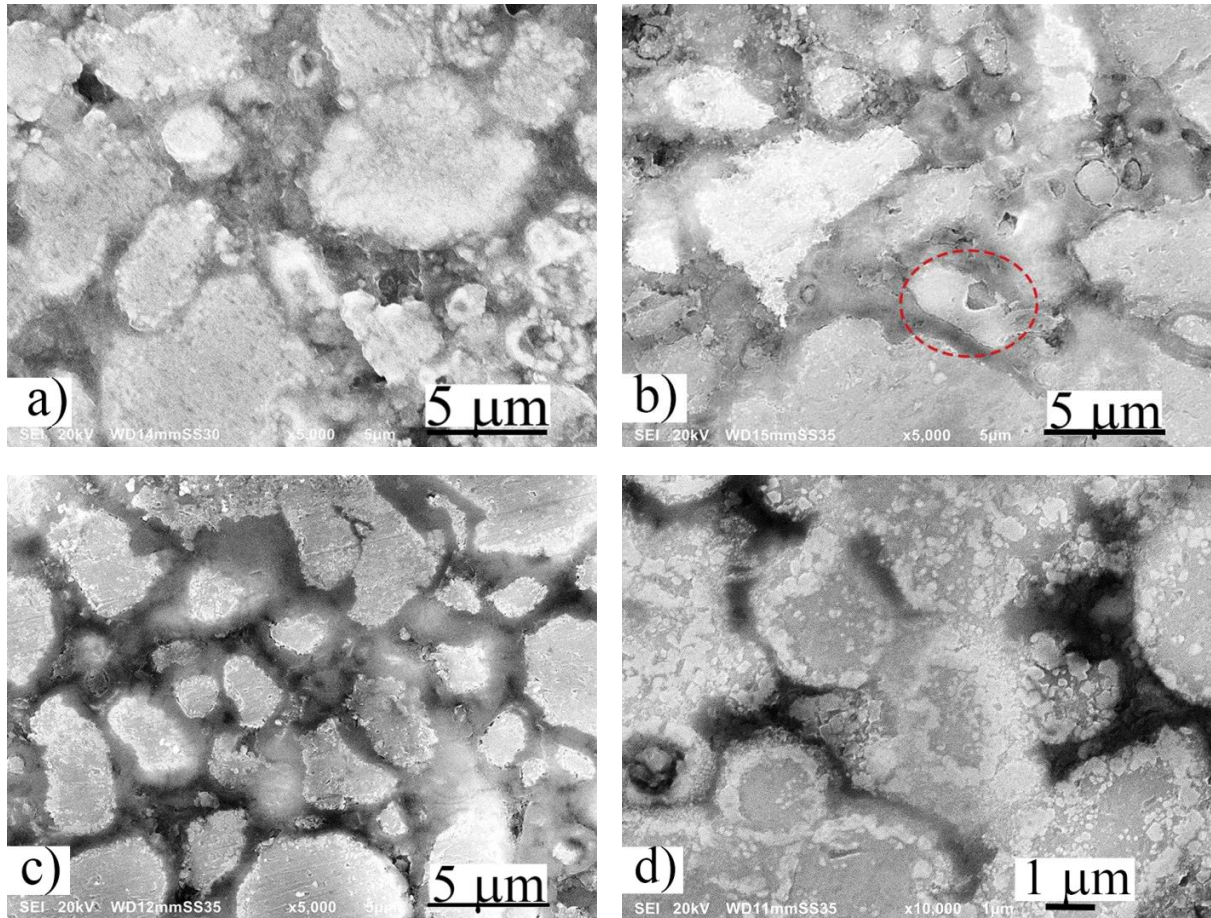
Fig. 4 SEM image of sintered composites (a) 0.2 wt.% rGO/Al (b) 0.4 wt.% rGO/Al (c) 0.6 wt.% rGO/Al (d) higher magnification of 0.6rGO/Al to reveal rGO on Al surface

TEM is employed to further study the microstructure of hybrid CNT-rGO interaction and adsorbed CNT-rGO on Al particle surface (Fig. 5a-d). The hybrid CNT-rGO composite in Fig. 5a reveal areas with CNT-rGO reticulate structure (red circles) and some isolated CNTs or rGO network (yellow circles). Clusters of rGO (Fig. 5b) observed on the Al surface can be attributed to large specific surface area of rGO and the Van der Waals forces [32]. Individual CNTs are linked by rGO sheets and with few CNT only network (Fig. 5c). In the high magnifation of the marked area (black square) in Fig. 5c, CNT wrapping of rGO on Al surface is revealed (Fig. 5d). The distribution of 1-D CNT and 2-D rGO is enhanced by formation of 3-D recticulate structure of the hybrid CNT-rGO reinforcement as revealed in the TEM images. Pressence of GO can reduce the agglomeration of CNTs through Van der Waals forces [30]. During the sonication of CNT and GO in water, the $\pi - \pi$ interaction between GO and CNTs promotes the dispersion of CNTs on GO surfaces (Fig. 1), forming hybrid reinforcement with reticulate structure [33,34].
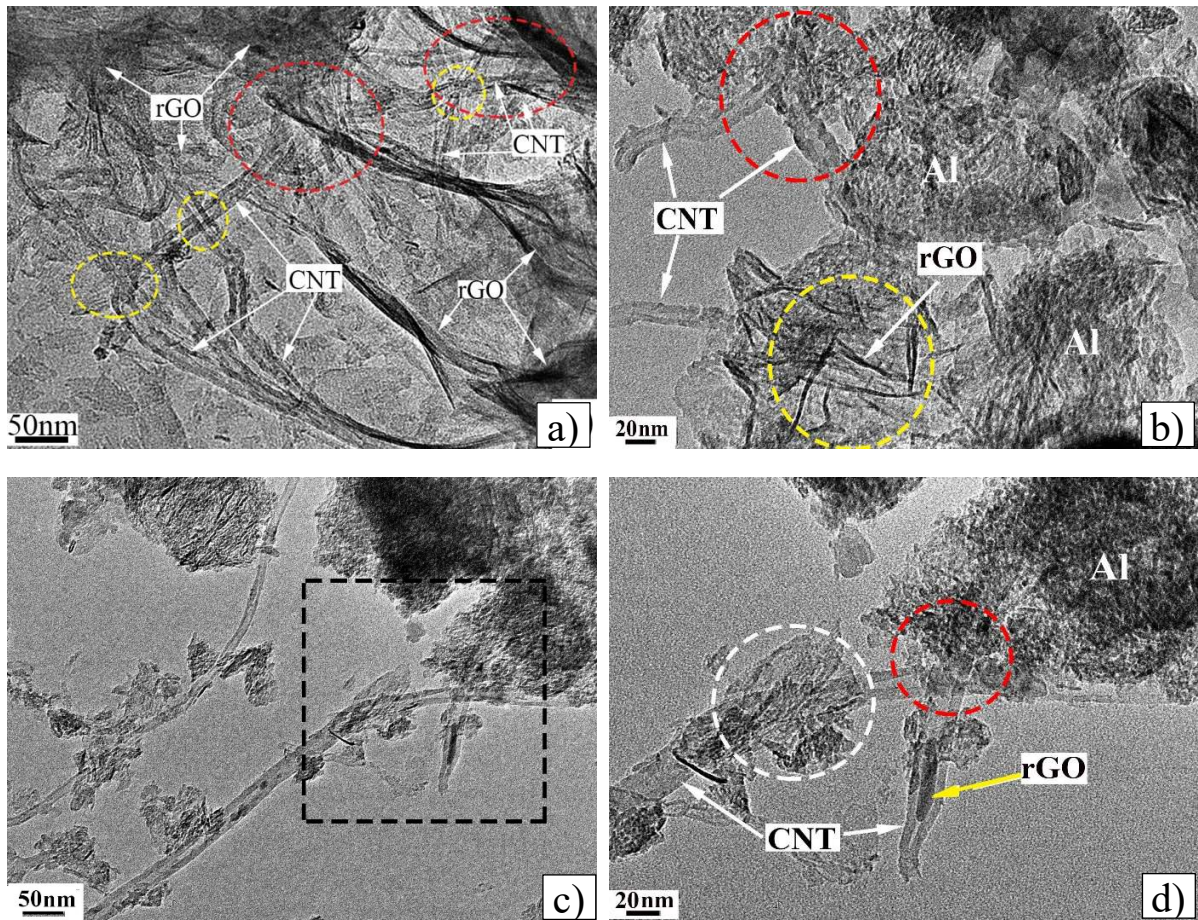
Fig. 5 TEM images of hybrid 0.2 wt.% CNT-rGO/Al composite after sintering showing: (a) CNTs network (b) Cohesion of rGO and CNTs to Al matrix, (c and d) wrapping of rGO and Al by CNTs, and (d) high magnification of the marked area in (c)

The XRD patterns of raw GO, CNT, pure Al, as well as composite powders of 0.6rGO/Al and CNT-rGO/Al(1:1) are shown in Fig. 6. Strong GO peak appears at $2\theta = 9.9°$ corresponding to the (001) basal plane with d-spacing (d_{001}) of 0.887 nm, which is consistent with XRD of GO reported previously [19]. The CNT powder gives a peak at $2\theta = 25.7°$, which indicates it's graphite like structure. The mixed powders however have peaks of 2θ equals to 38.3° (111), 44.5° (200), 64.9° (220) and 78.0° (311) corresponding to face-centered cubic (FCC) Al. The GO peak does not exist in neither the 0.6rGO/Al nor CNT-rGO/Al composite powders which indicates a reduction of GO during adsorption process [24,25].
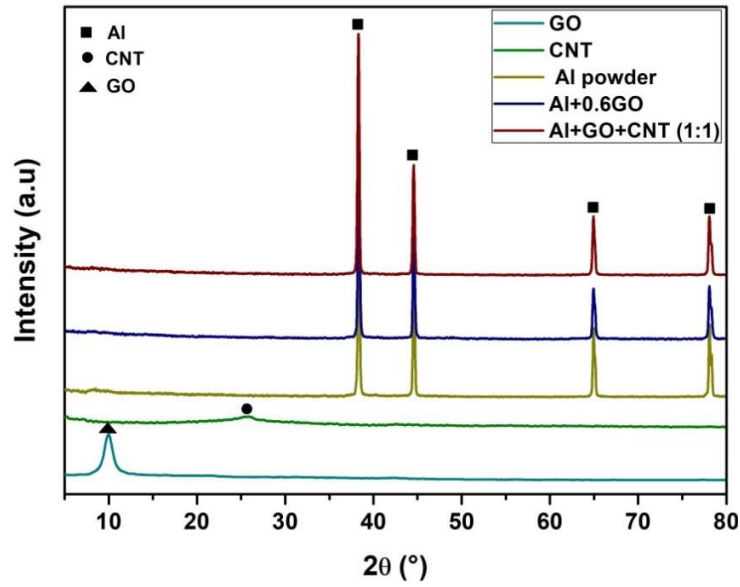
Fig. 6 XRD patterns of GO, CNT, pure Al, 0.6rGO/Al mixture and CNT-rGO/Al mixture powders

The XRD of sintered composites (Fig. 7), similar to the powder mixtures have strong peaks of 2θ equals to 38.3° (111), 44.5° (200), 64.9° (220) and 78.0° (311) corresponding to face-centered cubic (FCC) Al. The absence of second phases such as Al_3C_4 and Al_2O_3 suggest there is no damage to the rGO sheets and CNTs. This prevents the release of carbon and subsequent reaction with Al during sintering. Oxidation process was limited during the process due to the sintering of samples in a vacuum furnace [35]. The absence of Al_3C_4 can be attributed to processing method used and the careful selection of sintering temperature.
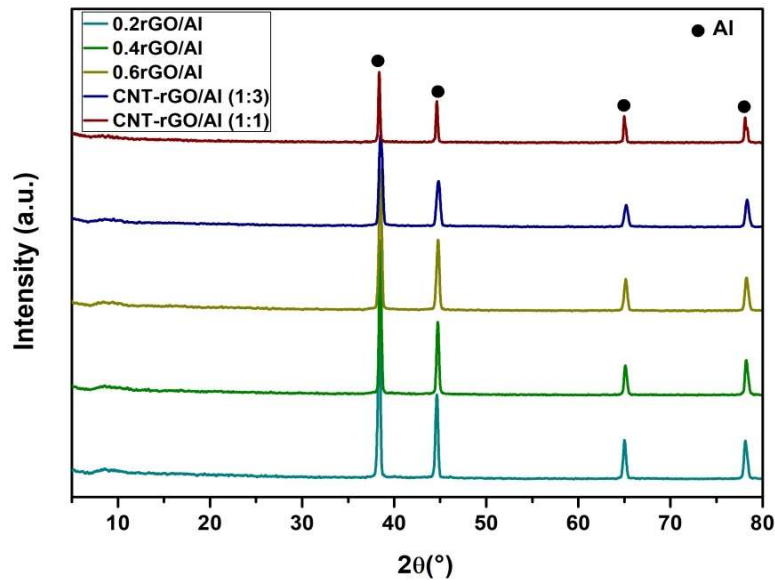

Fig. 7 XRD patterns of pure Al, 0.2rGO/Al, 0.4rGO/Al, 0.6rGO/Al and CNT-rGO/Al (ratios 1:1 and 1:3) sintered composite samples

3.2 Densification of composites

The density of rGO/Al composites slightly increased with 0.2 wt.% rGO addition reaching relative density of 97.3% but decreased with further increase in rGO content as presented in Fig. 8. The density of pure Al is affected by the presence of protective oxide layer on the particle surfaces of the as received powder [18]. The decrease in density on increasing rGO percentage above 0.2 wt.% can be explained by the diffusion of Al particles forming more continuous matrix at 0.2 wt.% but Al particles appear isolated (Fig. 4c) with further increase in reinforcement [18]. Hybrid composites have slightly higher relative density owing to the reduced mass fraction of rGO. Nano-sized reinforcement such as CNTs, effectively fills up microvoids at lower volume fractions increasing densification but turn to agglomerate at high volume fractions decreasing density [36]. Wettability problems and thermal expansion mismatch between Al and rGO create voids at the interface between matrix and reinforcement phase. This problem becomes more pronounced with increasing reinforcement mass fraction that causes the decreasing in the density values. Full densification by simple traditional compaction and sintering of rGO coated Al matrix composites is not possible. The tight rGO coating on Al particles acts as an internal barrier that restricts the interaction between particles [37].
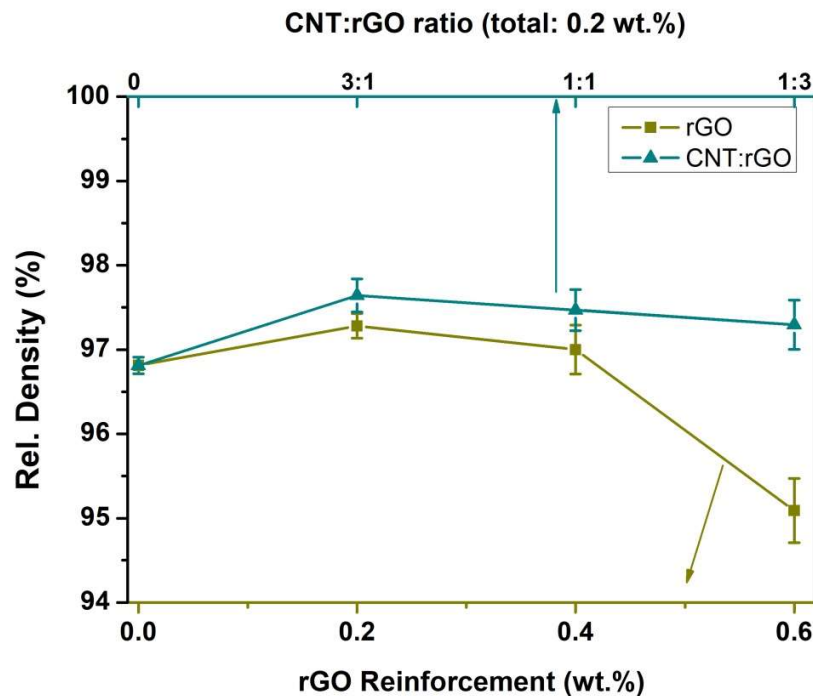

Fig. 8 Percentage densification of rGO and hybrid rGO-CNT coated Al matrix composites.

3.3 Mechanical properties

3.3.1 Hardness test

Vickers hardness test results are presented in Fig. 9a. The hardness values are 57.46 ± 2.7 HV, 82.91 ± 7 HV, 151.6 ± 6.2 HV, and 127.6 ± 8.1 HV for pure Al, 0.2 rGO/Al, 0.4 rGO/Al and 0.6 rGO/Al composites, respectively. These correspond to percentage increase in hardness values of composites over pure Al of 44.3%, 163.8% and 122% with rGO reinforcement of 0.2, 0.4, and 0.6 wt.%, respectively. The hardness increased with increasing rGO weight fraction up to 0.4 wt.% but declined at 0.6 wt.%. Similar trend was reported by Gao et al [38] and Zeng et al. [39] where hardness decreased when graphene wt.% is increased above 0.3, though the reason for the decline was not given. The decline in hardness may be attributed to the increased porosity of the samples with over 0.4 wt.% rGO, due to the non-wettability problem between rGO and Al. These results are in accordance with the density results. The hardness values (percentage increase over Al) for hybrid CNT-rGO/Al composites, as presented in Fig. 9b are 86.46 ± 4.1 HV (50.4%), 115.3 ± 4.5 HV (100.7%) and 88.14 ± 2.1 HV (53.4%) for composites with CNT:rGO ratio of 3:1, 1:1, 1:3 respectively. The total weight percentage of carbon nanofillers in all the hybrid composites is 0.2. Hybrid composite with CNT:rGO ratio of 1:1 recorded an increase in hardness value of 39.1% over rGO/Al composite with the same carbon nanofiller content (Fig. 9b). The hybrid composites in general, have a higher hardness values compared to rGO/Al with same total amount of reinforcement. Notably, the hybrid CNT-rGO reinforcement gives rise to synergistic improvement in hardness. The strong π-π interaction between rGO and CNT makes 1D CNT effectively bridge the 2D rGO sheets, which results in a 3D network of CNT-rGO/Al and provide significant improvement with low weight percent reinforcement [33,40]. The maximized synergistic effect according to the results is realized at-or-near the 1:1 stoichiometric ratio [41].

The improved hardness is due to many factors such as the presence of rGO nano sheets and CNT which have a high strength, grain refinement in which the rGO and CNT acts as an internal balls. This decrease the Al particle size that have a positive effect on the hardness values [37]. Also the good distribution of rGO and CNT in the Al matrix enhances the overall hardness. The presence of rGO coating which is difficult to deform, hinders the dislocation movement [42,43].
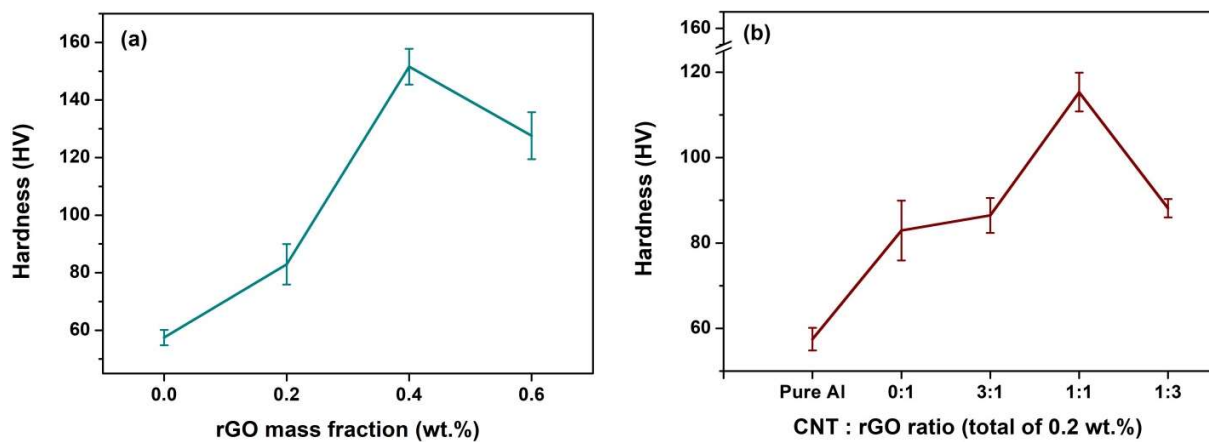

Fig. 9 Vickers Hardness of (**a**) rGO/Al composites (**b**) Hybrid CNT-rGO/Al composites

3.3.2 Wear resistance

The wear resistance of rGO and hybrid CNT-rGO reinforced Al composites is presented in Fig. 10(a-b). The wear rate (percentage reduction) of rGO/Al composites is 1.07 mg/s, 0.05 mg/s (95.3%), 0.023 mg/s (97.8%) and 0.262 mg/s (75.6%) for pure Al, 0.2 rGO/Al, 0.4 rGO/Al and 0.6 rGO/Al composites, respectively. The minimum wear rate is achieved at 0.4 wt.% rGO. The extraordinary improvement in wear resistance can be attributed to the increased hardness by rGO addition [43]. In addition, coating Al particles with rGO inhibits plastic deformation of the matrix at the contact surface. The excellent self-lubrication property of rGO [38] reduces friction at the contact surface thereby increasing wear resistance. The wear resistance declined at 0.6 wt.% due to increased porosity and thickness of rGO coating on Al particles, preventing proper consolidation during sintering. When the 'saturation' level of rGO is exceeded, there would be severe agglomeration of rGO. This can leads to degradation of the intrinsic mechanical properties of rGO sheets [11]. The increased layers of rGO sheets between Al particles cause aggregation of rGO, leading to reduced interfacial strength [16].
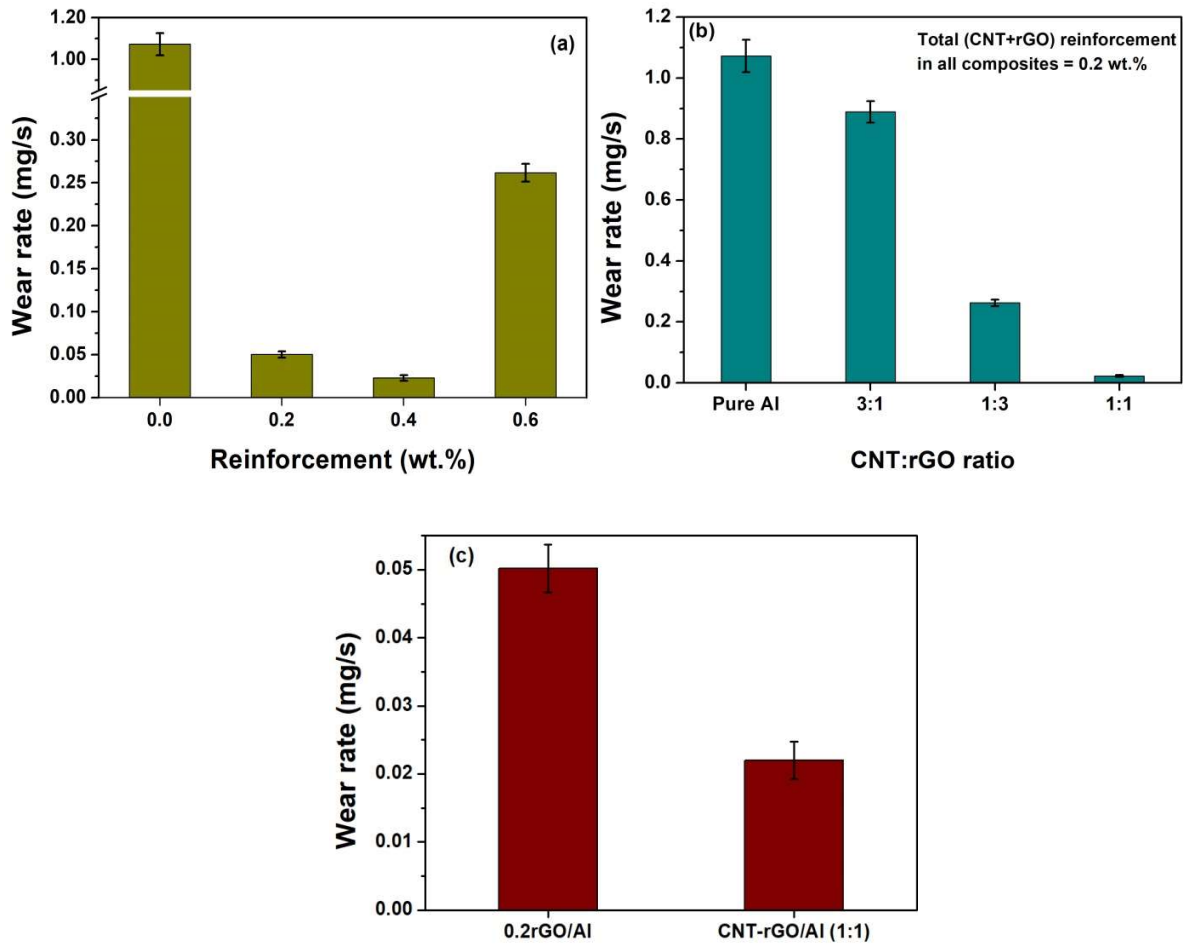

Fig. 10 (a) Wear rate of rGO/Al at different rGO reinforcement weight percent (b) Wear rate of Al matrix reinforced with total of 0.2 wt% CNT-rGO in different ratios (c) Comparison of 0.2 wt.% rGO and hybrid CNT-rGO (1:1) reinforced composites

Hybrid CNT-rGO reinforced composites with CNT:rGO ratio of 3:1, 1:3 and 1:1 recorded wear rate (percentage wear rate reduction compared to pure Al) of 0.889 mg/s (17.1%), 0.262 mg/s (75.6%) and 0.022 mg/s (97.9%), respectively. The wear resistance of the hybrid composites increased with increasing proportion of rGO. The maximum wear resistance is achieved with a ratio of 1:1 for the hybrid composites. In Fig. 10c, a comparison of wear rate of 0.2 wt.% rGO/Al composite and 0.2 wt.% hybrid CNT-rGO/Al (1:1) composite confirms the dominance of hybrid over rGO in wear resistance improvement. At 0.2 wt.% reinforcement, the hybrid CNT-rGO/Al (1:1) composite's wear rate is 56.1% lower than rGO/Al.

3.4 Coefficient of thermal expansion (CTE)

Fig. 11 shows the variation of the CTE of pure Al, rGO/Al and hybrid CNT-rGO/Al composites when temperature is increased from 150 to 350 °C. The CTE of rGO/Al composites decreased by approximately 5, 12 and 17% with addition of 0.2, 0.4 and 0.6 wt.% rGO, respectively. Hybrid composites' CTE decreased even further by approximately 21, 26 and 28% with addition of 0.2 wt% CNT-rGO in CNT:rGO ratios of 3:1, 1:3 and 1:1, respectively. Both CNT and rGO have been reported to reduce CTE of Al composites due to their very low intrinsic CTE (≈ 0 [44]). The reticulate network of CNT-rGO provides large surface area coverage and homogeneous dispersion of reinforcement in Al matrix. This provides a pinning effect at the boundaries of Al particles, thus constraining the expansion of Al particles during heating [45]. The linear decrease of CTE of pure Al with progressive addition of rGO is explained by the theory that thermal expansion of rGO coated Al composites is governed by the competing interactions between expansion of Al matrix and the constraint of rGO through their interfaces [45,46].
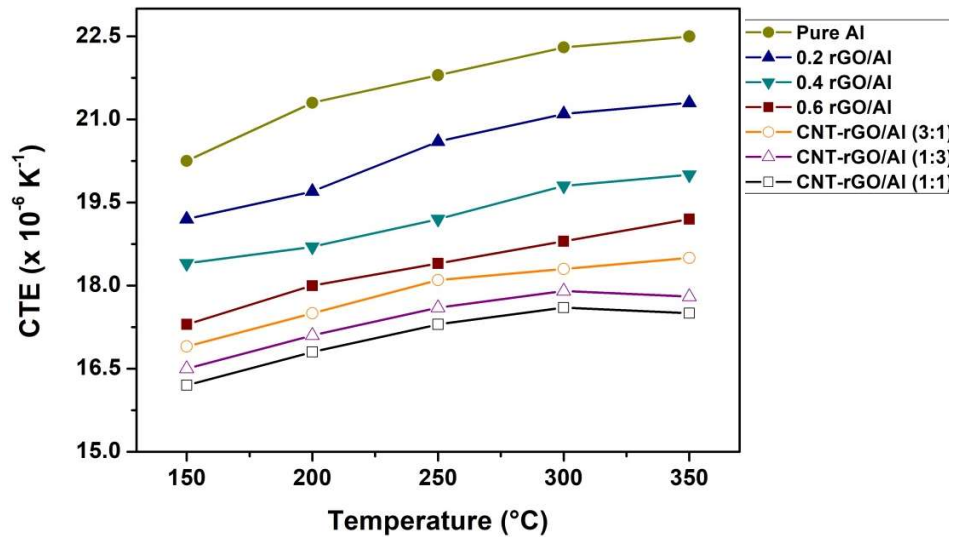

Fig. 11 CTE of pure Al, rGO/Al composites and hybrid CNT: rGO/Al measured from 150 °C to 350 °C

To study the influence of reinforcement on the CTE of the composites, theoretical models such as rule of mixture (ROM) (Eq. 2) and Turner's model (Eq. 3) for interconnected or continuous reinforcement [45,47,48] are often used to estimate the CTE of composites and compared with experimental results.

$$\varepsilon_c = \varepsilon_{rGO}V_{rGO} + \varepsilon_{Al}(100 - V_{rGO}) \tag{2}$$

$$\varepsilon_c = \frac{E_{rGO}\varepsilon_{rGO}V_{rGO} + E_{Al}\varepsilon_{Al}(100 - V_{rGO})}{E_{rGO}V_{rGO} + E_{Al}(100 - V_{rGO})} \tag{3}$$

where ε_c, ε_{rGO} (≈ 0.9 [49]) and ε_{Al} (≈ 22.5 [50]) are the CTE of rGO/Al composites, rGO and Al respectively; E_{rGO} (≈ 1 TPa [51]) and E_{Al} (≈ 69 GPa) are the elastic modulus of rGO and Al respectively; V_{rGO} is the rGO volume fraction. As shown in Fig. 12, there is no agreement between CTE values calculated by ROM and experimental values because ROM does not account for the complexity of reinforcement geometry and the interfacial thermal stress within the composite [47]. In sharp contrast, the Turner's model calculated values are in good agreement with experimental results (Fig. 12), deviating slightly at 0.6 wt.% rGO reinforcement. This model accounts for mechanical interaction between reinforcement and matrix phases but disregards shape and distribution factor of reinforcement particles within the composite, which is true for low volume fractions addition as used in this work [48]. The good fit between theoretical and experimental results can be attributed to the uniform dispersion, good bonding and tight continuous coating of rGO on Al particles, similar to the theoretical assumptions. However, as shown in earlier sections of this work, the linear relation between composite properties and reinforcement volume fraction breaks down at 0.6 wt.% due to possible agglomeration and porosity. The model CTE value is therefore 1.33% lower than experimental results for 0.6rGO/Al composite.
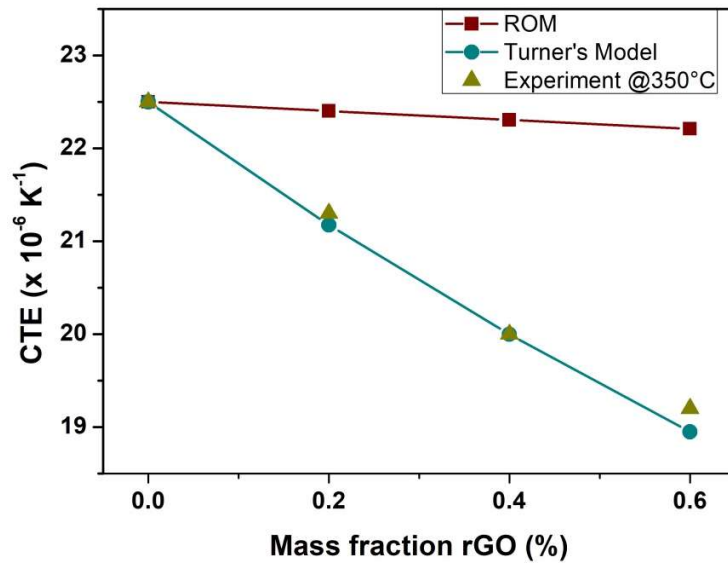

Fig. 12 Comparison between experimentally measured and theoretically calculated CTE versus rGO content of rGO/Al composites

3.5 Strengthening mechanism

The four main mechanisms likely to be associated with strengthening efficiency of carbon nanofiller reinforcement are grain refinement, Orowan strengthening, load transfer and thermal expansion mismatch [30]. In rGO/Al composites, the tight coating of rGO on Al particles due to electrostatic interaction and the low thermal expansion of rGO, makes Orowan looping one of the most important strengthening mechanism [52]. The significant mismatch between the CTE of Al matrix and carbon nanofillers generates dislocations. The increased dislocation density in the matrix leads to composite strengthening [53].The high intrinsic strength of graphene (rGO) enables it to hinder dislocation movement across grain boundaries. On further plastic deformation, back stress is produced by dislocation loops formed around the rGO, thus increasing resistance to dislocation flow and increased strength of the composite. Hindrance to dislocation movement on the other hand results in reduction in ductility. RGO strengthening of Al matrix is predominantly through hindering the flow of dislocation and not load transfer from matrix to reinforcement [54].

In case of hybrid CNT-rGO/Al composites, individual CNTs are connected by rGO sheets through π-π interaction to form a reticulate structure on surface of Al particles. The main form of strengthening mechanism in CNT reinforced composites is load transfer [32] for high aspect ratios. The rGO interconnection increases the available surface area for load transfer and also enables the CNT-rGO reticulate structure to deform as a whole, leading to enhanced load transfer capabilities [11]. The improvement in the mechanical properties of hybrid CNT-rGO/Al composites is thus attributed to both Orowan strengthening and significant load transfer mechanisms as opposed to only Orowan strengthening dominant in rGO/Al composites. The low mass fraction of CNT-rGO reinforcement (0.2 wt.%) studied in this work also eliminate most of the loss in intrinsic mechanical properties associated with rGO and CNT agglomeration.

The composite strengthening mechanism is expressed as [56]:

$$\sigma_c = (1 + 0.5V_r)\left(\sigma_{Al} + \sigma_{CTE} + \sigma_{Orowan} + \frac{\sigma_{Orowan}\sigma_{CTE}}{\sigma_{Al}}\right) \qquad (4)$$

where

$$\sigma_{CTE} = 1.25Gb\sqrt{\frac{12\Delta T \Delta C V_r}{bd_p}} \qquad (5)$$

$$\sigma_{Orowan} = 0.13Gb\frac{\ln\left(d_p/2b\right)}{d_p\left[\left(1/2V_r\right)^{1/3}-1\right]} \qquad (6)$$

Where σ_c = yield strength contribution calculated from Orowan strengthening mechanism, σ_{Al} = yield strength of Al matrix (84.6 MPa), σ_{CTE} = thermal expansion mismatch contribution to increase in yield strength, σ_{Orowan} = increase in yield strength from Orowan looping around reinforcement, G = shear modulus of Al (26.9 GPa), b = Burger's vector of Al (0.286 nm), ΔT = difference between sintering and testing temperature (575 °C), ΔC = difference between CTE of Al (22.6 x 10^{-6} K^{-1}) and rGO/CNT (0.9 x 10^{-6} K^{-1}), V_r = volume fraction of reinforcement and d_p = effective reinforcement diameter.

For rGO/Al and CNT-rGO/Al composites, d_p is estimated by assuming a spherical model for rGO and CNT. Therefore the d_p of rGO and CNT-rGO are given by the following equations, respectively.

$$d_{p(rGO)} = \sqrt[3]{\frac{3wtl}{4\pi}}, \tag{7}$$

$$d_{p(CNT-rGO)} = \sqrt[3]{\frac{3(wtl+xSl_{CNT})}{4\pi}} \tag{8}$$

Where S and l_{CNT} are cross sectional area and length of CNT respectively; w, t and l are the width, thickness and length of rGO and x (=1,2,3...) is the quantity of CNTs in hybrid [57]. In addition, the CNTs in the hybrid composite enable load transfer strengthening [58]. The load transfer contribution to increase in yield strength can be expressed by the modified shear-lag equation as [48]:

$$\Delta\sigma_{LT} = pV_r\sigma_{Al} \tag{9}$$

where p is aspect ratio of reinforcement

The strengthening mechanisms of the fabricated composites after sintering at 600 °C for 1 hr are summarized in Table 1. It is obvious that CNT-rGO reinforcements increase the yield strength by increasing volume fraction and by minimum 31% at 0.2 wt.% reinforcement

Table 1 Contributions of the strengthening mechanisms of the studied composites

Composite	Volume fraction (wt.%)	Strengthening Mechanism (MPa)			
		Orowan (σ_{Orowan})	CTE mismatch (σ_{CTE})	Load transfer (σ_{LT})	Total Contribution (σ_C)
rGO/Al	0.2	0.383	33.8	0.0038	119.17
	0.4	0.786	47.7	0.0076	134.10
	0.6	1.210	58.3	0.0113	145.96
CNT-rGO/Al (1:1)	0.2	0.469	33.5	37.985	157.09
	0.4	0.961	47.3	75.717	210.05
	0.6	1.480	57.9	113.364	260.06

Conclusions:

Al reinforced with rGO (0.2, 0.4 and 0.6 wt.%) and hybrid CNT-rGO (CNT:rGO ratios of 3:1, 1:1 and 1:3) is fabricated successfully by solution coating powder metallurgy. The microstructure, density, hardness, wear resistance and CTE of the composite are investigated. The following conclusions can be drawn from the study:

- GO and hybrid CNT-GO can be homogeneously dispersed in Al matrix by adsorption of GO on Al particles by electrostatic self-assembly of GO on Al particles leading to in-situ reduction of GO.

- The hardness of rGO/Al composites is increased with increasing rGO mass fraction up to 0.4 wt.% but declined with further increased of reinforcement to 0.6 wt.%. The maximum percentage increase in hardness of rGO/Al composites over Al sample is 163.8% with rGO reinforcement of 0.4 wt.%. Hardness of hybrid CNT-rGO/Al composites with CNT:rGO ratio of 1:1 increased by 100.7% and 39.1% over Al samples and rGO/Al composite with same 0.2 wt.% reinforcement, respectively.

- The wear rate of Al composites reduced drastically by a minimum of 75.6% and maximum of 97.3%. The hybrid CNT-rGO/Al (1:1) composite's wear rate is 56.1% lower than rGO/Al of same carbon nanofiller content, thus showing synergistic reinforcement between CNT and rGO in Al matrix at-or-near the stoichiometric ratio of 1:1.

- The CTE of composites generally decreased with increasing rGO content up to 17% and as low as 28% in hybrid composites.

Acknowledgement

Conflict of interest:

The authors declare that they have no conflict of interest.

References

[1] P. Hidalgo-Manrique, S. Yan, F. Lin, Q. Hong, I.A. Kinloch, X. Chen, R.J. Young, X. Zhang, S. Dai, Journal of Materials Science 52 (2017) 13466–13477.

[2] A.A. Adebisi, M.A. Maleque, M.M. Rahman, International Journal of Automotive and Mechanical Engineering 4 (2011) 471–480.

[3] Y. Wang, P. Shen, R.-F. Guo, Z.-J. Hu, Q.-C. Jiang, Ceramics International 43 (2017) 3831–3838.

[4] I.-J. Shon, Ceramics International 42 (2016) 17884–17891.

[5] C. Ye, X. Yue, Y. Jiang, H. Li, H. Ru, Ceramics International 44 (2018) 3664–3671.

[6] O. El-Kady, A. Fathy, Materials & Design (1980-2015) 54 (2014) 348–353.

[7] J.A. Rodríguez-González, C. Rubio-González, M. Jiménez-Mora, L. Ramos-Galicia, C. Velasco-Santos, Applied Composite Materials 25 (2018) 1115–1131.

[8] Y.-F. Chen, Y.-J. Tan, J. Li, Y.-B. Hao, Y.-D. Shi, M. Wang, Polymer Testing 65 (2018) 387–397.

[9] X. Zhang, W. Yang, J. Zhang, X. Ge, X. Liu, Y. Zhan, Materials Science and Engineering: A 743 (2019) 512–519.

[10] I.-J. Shon, J.-K. Yoon, K.-T. Hong, Metals and Materials International 24 (2018) 130–135.

[11] Z. Li, G. Fan, Q. Guo, Z. Li, Y. Su, D. Zhang, Carbon 95 (2015) 419–427.

[12] M. Bastwros, G.-Y. Kim, C. Zhu, K. Zhang, S. Wang, X. Tang, X. Wang, Composites Part B: Engineering 60 (2014) 111–118.

[13] S.E. Shin, H.J. Choi, J.H. Shin, D.H. Bae, Carbon 82 (2015) 143–151.

[14] J. Wang, Z. Li, G. Fan, H. Pan, Z. Chen, D. Zhang, Scripta Materialia 66 (2012) 594–597.

[15] M. Rashad, F. Pan, A. Tang, M. Asif, Progress in Natural Science: Materials International 24 (2014) 101–108.

[16] H. Kwon, J. Mondal, K.A. AlOgab, V. Sammelselg, M. Takamichi, A. Kawaski, M. Leparoux, Journal of Alloys and Compounds 698 (2017) 807–813.

[17] X. Gao, H. Yue, E. Guo, H. Zhang, X. Lin, L. Yao, B. Wang, Materials & Design 94 (2016) 54–60.

[18] Z. Baig, O. Mamat, M. Mustapha, A. Mumtaz, M. Sarfraz, S. Haider, Metals 8 (2018) 90.

[19] D. Li, Y. Ye, X. Liao, Q.H. Qin, Nano Research 11 (2018) 1642–1650.

[20] X. Gao, H. Yue, E. Guo, H. Zhang, X. Lin, L. Yao, B. Wang, Materials & Design 94 (2016) 54–60.

[21] T. He, X. He, P. Tang, D. Chu, X. Wang, P. Li, Materials & Design 114 (2017) 373–382.

[22] E. Ghasali, P. Sangpour, A. Jam, H. Rajaei, K. Shirvanimoghaddam, T. Ebadzadeh, Archives of Civil and Mechanical Engineering 18 (2018) 1042–1054.

[23] H.-C. Youn, S.-M. Bak, S.-H. Park, S.-B. Yoon, K.C. Roh, K.-B. Kim, Metals and Materials International 20 (2014) 975–981.

[24] L. Zhang, G. Hou, W. Zhai, Q. Ai, J. Feng, L. Zhang, P. Si, L. Ci, Journal of Alloys and Compounds 748 (2018) 854–860.

[25] Z. Fan, K. Wang, T. Wei, J. Yan, L. Song, B. Shao, Carbon 48 (2010) 1686–1689.

[26] Z. Li, G. Fan, Z. Tan, Q. Guo, D. Xiong, Y. Su, Z. Li, D. Zhang, Nanotechnology 25 (2014) 325601.

[27] S.C. Tjong, Materials Science and Engineering: R: Reports 74 (2013) 281–350.

[28] M.A. Rafiee, J. Rafiee, Z. Wang, H. Song, Z.-Z. Yu, N. Koratkar, ACS Nano 3 (2009) 3884–3890.

[29] H.M. Yehia, O.A. Elkady, Y. Reda, K.E. Ashraf, Transactions of the Indian Institute of Metals 72 (2019) 85–92.

[30] X. Zhang, C. Shi, E. Liu, F. He, L. Ma, Q. Li, J. Li, N. Zhao, C. He, Composites Part A: Applied Science and Manufacturing 103 (2017) 178–187.

[31] Z.Y. Liu, S.J. Xu, B.L. Xiao, P. Xue, W.G. Wang, Z.Y. Ma, Composites Part A: Applied Science and Manufacturing 43 (2012) 2161–2168.

[32] X. Chen, J. Tao, J. Yi, Y. Liu, C. Li, R. Bao, Materials Science and Engineering: A 718 (2018) 427–436.

[33] J.-K. Wu, C.-C. Ye, T. Liu, Q.-F. An, Y.-H. Song, K.-R. Lee, W.-S. Hung, C.-J. Gao, Materials & Design 119 (2017) 38–46.

[34] C. Subramaniam, T. Yamada, K. Kobashi, A. Sekiguchi, D.N. Futaba, M. Yumura, K. Hata, Nature Communications 4 (2013).

[35] Z. Baig, O. Mamat, M. Mustapha, Critical Reviews in Solid State and Materials Sciences 43 (2018) 1–46.

[36] S.N. Alam, L. Kumar, Materials Science and Engineering: A 667 (2016) 16–32.

[37] M.M.M. Mohammed, O.A. Elkady, A.W. Abdelhameed, Open Journal of Metal 03 (2013) 72–79.

[38] X. Gao, H. Yue, E. Guo, S. Zhang, B. Wang, E. Guan, S. Song, H. Zhang, Materials Science and Technology (2018) 1–7.

[39] X. Zeng, J. Teng, J. Yu, A. Tan, D. Fu, H. Zhang, International Journal of Minerals, Metallurgy, and Materials 25 (2018) 102–109.

[40] Y. Pan, H. Bao, L. Li, ACS Applied Materials & Interfaces 3 (2011) 4819–4830.

[41] M. Yadav, K.Y. Rhee, S.J. Park, Carbohydrate Polymers 110 (2014) 18–25.

[42] J. Liu, U. Khan, J. Coleman, B. Fernandez, P. Rodriguez, S. Naher, D. Brabazon, Materials & Design 94 (2016) 87–94.

[43] R. Pérez-Bustamante, D. Bolaños-Morales, J. Bonilla-Martínez, I. Estrada-Guel, R. Martínez-Sánchez, Journal of Alloys and Compounds 615 (2014) S578–S582.

[44] H. Kwon, D.H. Park, J.F. Silvain, A. Kawasaki, Composites Science and Technology 70 (2010) 546–550.

[45] P.R. Matli, F. Ubaid, R.A. Shakoor, G. Parande, V. Manakari, M. Yusuf, A.M. Amer Mohamed, M. Gupta, RSC Advances 7 (2017) 34401–34410.

[46] P. Sharma, S. Sharma, D. Khanduja, Journal of Asian Ceramic Societies 3 (2015) 240–244.

[47] M.P. Reddy, M.A. Himyan, F. Ubaid, R.A. Shakoor, M. Vyasaraj, P. Gururaj, M. Yusuf, A.M.A. Mohamed, M. Gupta, Ceramics International (2018).

[48] P.V. Trinh, N.V. Luan, D.D. Phuong, P.N. Minh, A. Weibel, D. Mesguich, C. Laurent, Composites Part A: Applied Science and Manufacturing 105 (2018) 126–137.

[49] J.S. Bunch, (2008).

[50] H. Ji, R. Mclendon, J.A. Hurtado, V. Oancea, J. Bi, (2018) 26.

[51] H. Kwon, M. Estili, K. Takagi, T. Miyazaki, A. Kawasaki, Carbon 47 (2009) 570–577.

[52] R.J. Arsenault, N. Shi, Materials Science and Engineering 81 (1986) 175–187.

[53] W.J. Kim, Y.J. Yu, Scripta Materialia 72–73 (2014) 25–28.

[54] A. Bisht, M. Srivastava, R.M. Kumar, I. Lahiri, D. Lahiri, Materials Science and Engineering: A 695 (2017) 20–28.

[55] M. Yang, L. Weng, H. Zhu, F. Zhang, T. Fan, D. Zhang, Scientific Reports 7 (2017).

[56] B. Chen, J. Shen, X. Ye, L. Jia, S. Li, J. Umeda, M. Takahashi, K. Kondoh, Acta Materialia 140 (2017) 317–325.

[57] A. Kelly, W. Tyson, J Mech Phy Solids 13 (1965) 329–350.

[58] M. Steen, J.-L. Vallés, Materials Science and Engineering: A 250 (1998) 217–221.